

# Purcell enhanced optical refrigeration

Peng Ju,<sup>1</sup> Stefan Püschel,<sup>2</sup> Kunhong Shen,<sup>1</sup> Yuanbin Jin,<sup>1</sup> Hiroki Tanaka,<sup>2</sup> and Tongcang Li,<sup>1,3,4,5,\*</sup>

<sup>1</sup>*Department of Physics and Astronomy, Purdue University, West Lafayette, Indiana 47907, USA*

<sup>2</sup>*Leibniz-Institut für Kristallzüchtung (IKZ), Max-Born-Str. 2, Berlin 12489, Germany*

<sup>3</sup>*Elmore Family School of Electrical and Computer Engineering,  
Purdue University, West Lafayette, Indiana 47907, USA*

<sup>4</sup>*Birck Nanotechnology Center, Purdue University, West Lafayette, Indiana 47907, USA and*

<sup>5</sup>*Purdue Quantum Science and Engineering Institute,  
Purdue University, West Lafayette, Indiana 47907, USA*

(Dated: May 1, 2024)

Optical refrigeration of solids with anti-Stokes fluorescence has been widely explored as a vibration-free cryogenic cooling technology. A minimum temperature of 87 K has been demonstrated with rare-earth ion doped crystals using optical refrigeration. However, the depletion of the upper-lying energy levels in the ground state manifold hinders further cooling to below liquid nitrogen (LN<sub>2</sub>) temperatures, confining its applications. In this work, we introduce a Purcell enhanced optical refrigeration method to circumvent this limitation. This approach enhances the emission of high energy photons by coupling to a nearby nanocavity, blue shifting the mean emission wavelength. Such Purcell enhanced emission facilitates cooling starting from a lower energy level in the ground state manifold, which exhibits a higher occupation below LN<sub>2</sub> temperatures. Using our experimentally measured optical coefficients, our theoretical analysis predicts a minimum achievable temperature of 38 K for a Yb<sup>3+</sup>:YLiF<sub>4</sub> nanocrystal near a cavity under realistic conditions. The proposed method is applicable to other rare-earth ion doped materials and semiconductors, and will have applications in creating superconducting and other quantum devices with solid-state cooling.

Optical refrigeration of solids, as a vibration-free and highly reliable cooling method, has made great progress over the last few decades [1, 2]. Since the first demonstration of fluorescence cooling [3], optical refrigeration has been applied to directly cool semiconductors [4] and various rare-earth ion doped crystals [5–7] as well as nanocrystals [8]. Efficient fluorescence cooling is also proposed to reduce the temperature of quantum devices [9]. Besides the study of intrinsic cooling, optical refrigeration has been successfully applied to several research domains. Target devices such as mechanical resonators [10], quantum defects in diamonds [11], and infrared sensors [12, 13] are thermally attached to Yb<sup>3+</sup> doped crystals and indirectly cooled. Moreover, optical refrigeration can cool both the internal temperature and center-of-mass motion of an optically levitated Yb<sup>3+</sup> doped nanocrystal [8, 14–16], with the potential for precision measurement [17] and studying macroscopic quantum effects [18].

The state-of-art optical refrigeration is demonstrated with Yb<sup>3+</sup> doped YLiF<sub>4</sub> (YLF) crystals, achieving a record low temperature of 87 K [19, 20]. To maximize the cooling efficiency, the Yb<sup>3+</sup> ions are resonantly pumped from highest ground-state to the lowest excited-state Stark level. However, the cooling efficiency diminishes due to the population depletion of the absorbing level as temperature reduces and is eventually dominated by parasitic absorption below 100 K. The limit on the minimum achievable temperature (MAT) prevents several potential applications using optical refrigeration, including studying high-T<sub>c</sub> superconductivity [21] and quantum defects in 2D materials [22], which require the internal temperature to be lower than the liquid nitrogen (LN<sub>2</sub>) tem-

perature. While the parasitic absorption can be mitigated using higher purity host crystals, the implication and practical viability of this approach remains to be investigated [19].

The emission rate of an emitter can be affected by the electromagnetic density of states at the emission frequency, known as Purcell effect [23, 24]. Purcell factor ( $F_p$ ) quantifies the enhancement ratio of an emitter over the intrinsic spontaneous emission due to Purcell effect. For an electric or magnetic dipole resonantly coupled to a cavity mode,  $F_p = \frac{3\lambda_n^3}{4\pi^2} \frac{Q}{V_m}$ , where  $\lambda_n$  is the wavelength in the material with a refractive index  $n$ ,  $Q$  is the quality factor of the mode, and  $V_m$  is the effective mode volume. Recently, cavities with high  $F_p$  have been applied to increase the emission rate of rare-earth ions [25, 26] and atoms [27, 28] near a photonic cavity. Inspired by these experiments, we propose a novel protocol to significantly enhance optical refrigeration with cavity-induced Purcell effect and reduce the MAT of a Yb<sup>3+</sup> doped YLF nanocrystal well below the LN<sub>2</sub> temperature. In the protocol, the Purcell effect selectively enhances high-energy fluorescence photon emission, causing a blueshift of the mean emission wavelength, thereby enabling the pumping of stronger absorption lines at shorter wavelengths, which remain pertinent for anti-Stokes fluorescence. Based on our experimentally measured absorption and fluorescence spectra, we predict a MAT of 38 K for a Yb<sup>3+</sup>:YLF nanocrystal near a nanocavity using our proposed optical refrigeration approach.

A schematic diagram of our proposed Purcell enhanced optical refrigeration is shown in Fig. 1(a). A 5% Yb<sup>3+</sup>:YLF nanocrystal is located near a photonic cav-

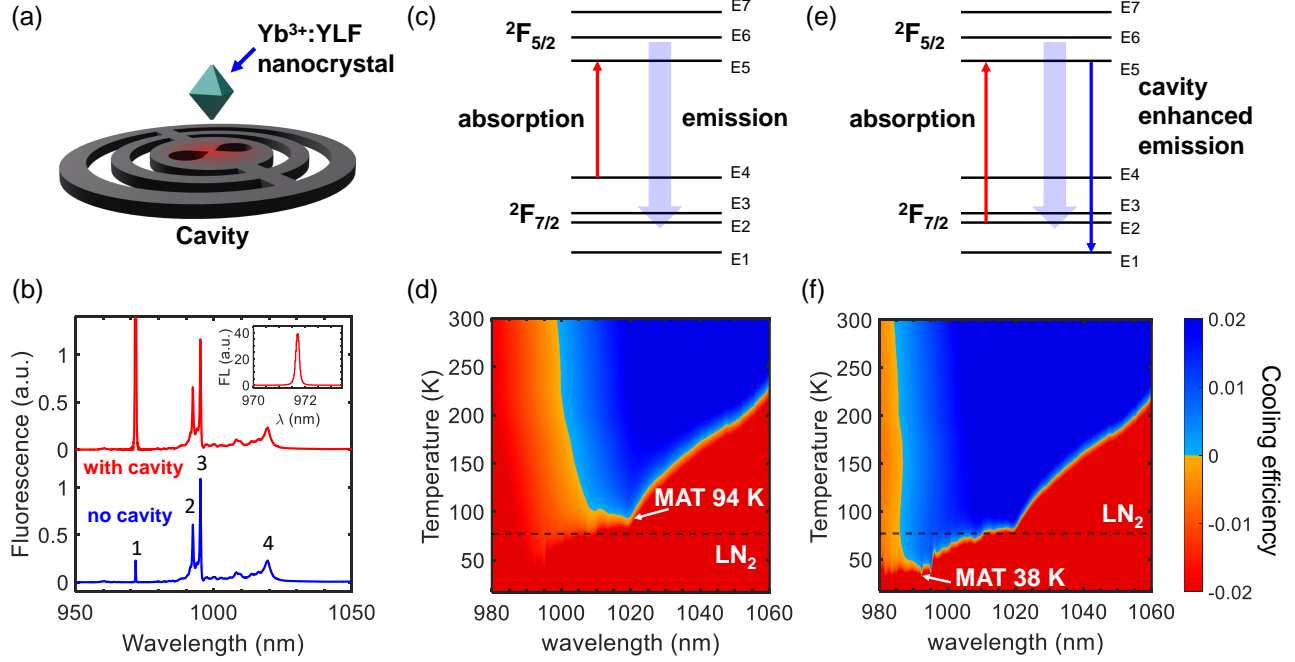


FIG. 1. Purcell enhanced optical refrigeration of a  $\text{Yb}^{3+}:\text{YLF}$  nanocrystal near a photonic nanocavity. (a) Schematic diagram of Purcell enhanced optical refrigeration protocol. The emission of high energy photon from  $\text{Yb}^{3+}:\text{YLF}$  nanocrystal is enhanced by a bowtie-shaped photonic nanocavity. The nanocrystal and nanocavity are separated by a vacuum. (b) Pi-polarized emission spectrum of  $\text{Yb}^{3+}:\text{YLF}$  nanocrystal with (top red) and without (bottom blue) a nearby nanocavity at 50 K. The four labeled peaks of the blue curve correspond to resonant transitions from E5 to E1, E2, E3 and E4. The inset shows the Purcell enhanced emission peak near 972 nm. (c) Energy diagram of the  $\text{Yb}^{3+}:\text{YLF}$  nanocrystal and the conventional optical refrigeration protocol with natural spontaneous emission.  $\text{Yb}^{3+}:\text{YLF}$  nanocrystal absorbs 1020 nm photons and emits a broadband fluorescence determined by the branching ratio. (d) Cooling efficiency as a function of temperature and pump wavelength without the cavity. The minimum achievable temperature (MAT) without Purcell enhancement is 94 K when pumped with 1020 nm laser. The horizontal black dashed line indicates the  $\text{LN}_2$  temperature at 77 K. (e) Energy diagram of Purcell enhanced optical refrigeration of a  $\text{Yb}^{3+}:\text{YLF}$  nanocrystal near a nanocavity. The nanocrystal is pumped with 992 nm laser, represented by solid red arrow. The Purcell enhanced emission is dominated by the resonant transition from E5 to E1, represented as solid blue arrow, in addition to the intrinsic spontaneous emission. (f) Cooling efficiency as a function of temperature and pump wavelength with the cavity. The MAT for Purcell enhanced optical refrigeration of  $\text{Yb}^{3+}:\text{YLF}$  nanocrystal is 38 K when pumped with 992 nm laser, well below the  $\text{LN}_2$  temperature.

ity, which increases the local density of the photonic states and selectively enhances the emission rate of the nanocrystal around the cavity resonant wavelength by the Purcell effect. The cooling efficiency ( $\eta_c$ ) of the  $\text{Yb}^{3+}:\text{YLF}$  nanocrystal is given by [1]:

$$\eta_c(T, \lambda) = \eta_{\text{ext}} \eta_{\text{abs}}(T, \lambda) \frac{\lambda}{\tilde{\lambda}(T)} - 1 \quad (1)$$

Here,  $\eta_{\text{ext}}$  is the external quantum efficiency of  $\text{Yb}^{3+}$ , which takes into account non-radiative decay, the fluorescence trapping, and re-absorption.  $\eta_{\text{ext}}$  is mainly determined by the property of the nanocrystal and we assume it is independent of temperature for simplicity.  $\lambda$  is the wavelength of the absorbed photons and  $T$  is the temperature of the nanocrystal.  $\tilde{\lambda}(T)$  is the mean emission wavelength at  $T$ .  $\tilde{\lambda}(T)$  depends on the Purcell effect which affects emission spectra.  $\eta_{\text{abs}}(T, \lambda) =$

$[1 + \alpha_b/\alpha(T, \lambda)]^{-1}$  is the absorption efficiency of the  $\text{Yb}^{3+}$ , where  $\alpha_b$  is parasitic background absorption and  $\alpha(T, \lambda)$  is the absorption coefficient of pumping laser.

In the proposed method, the cavity tailored to enhance emission at the zero phonon line reduces the mean emission wavelength, thereby increases cooling efficiency. The  $\text{Yb}^{3+}:\text{YLF}$  nanocrystal and photonic cavity are separated by vacuum. Such a design minimizes the thermal contact between them while achieves strong light-matter interaction depending on the separation. Experimentally, this can be achieved by either near-field optical levitation of the nanocrystal [29, 30] or bringing a nanocrystal attached to a nanotube [31] near the cavity. For near-field optical levitation, the trapping laser can simultaneously serve as the cooling laser.

To accurately evaluate the performance of the proposed optical refrigeration method, we measured the intrinsic fluorescence spectra of a bulk  $\text{Yb}^{3+}:\text{YLF}$  crystal,

with a care to minimize the re-absorption [32], for a temperature range of 20 to 300 K. These can serve as accurate approximations for the fluorescence spectra of  $\text{Yb}^{3+}:\text{YLF}$  nanocrystals. The blue curve in Fig. 1(b) shows the measured pi-polarized fluorescence spectrum at 50 K. The four peaks corresponding to the inter-Stark-level transitions are labeled based on their terminating level according to the energy diagram of  $\text{Yb}^{3+}$  in YLF shown in Fig. 1(c). To minimize  $\tilde{\lambda}(T)$  and, consequently, improve cooling efficiency, the cavity is designed to be resonant with the zero-phonon emission peak at 971.6 nm (Peak 1), which has the highest photon energy among the major four peaks in the emission spectrum.

The enhancement ratio for the emission near the wavelength of the cavity mode is determined by both the  $F_p$  at the position of the nanocrystal and the linewidth of the cavity. The bowtie design of photonic cavity confines the photons in a deep sub-wavelength mode-volume, inducing strong light-matter interaction near the center of the cavity. With topology-optimized design, such cavities have experimentally demonstrated  $F_p = 6 \times 10^3$  for a linewidth of 2 nm at the center of the cavity [33, 34]. In our protocol, we assume the same cavity linewidth and a moderate  $F_p$  of 180 at the location of the  $\text{Yb}^{3+}:\text{YLF}$  nanocrystal. This corresponds to a cavity quality factor ( $Q$ ) of 1100. The emission spectrum with cavity-induced Purcell enhancement is calculated based on above parameters, shown as the red curve in Fig 1. (b). Compared to the spectrum without cavity (blue curve), the mean emission wavelength is blue shifted from 1004 nm to 982 nm as the cavity selectively enhanced the emission of high energy (short wavelength) photons, shown in Fig. S1(b). This enhances the cooling efficiency of  $\text{Yb}^{3+}:\text{YLF}$  nanocrystal by nearly a factor of 2 assuming the same pump wavelength. In addition to the enhanced cooling power, blueshift of the mean emission wavelength extends the wavelength for cooling ( $\lambda > \tilde{\lambda}$ ) and allows us to utilize stronger absorption lines to improve the pump absorption.

Fig. 1(c) shows the energy level of the  $\text{Yb}^{3+}$  and the traditional optical refrigeration method. The  $\text{Yb}^{3+}$  is pumped with 1020 nm photons, which is the center wavelength of peak 4 shown in Fig. 1(b). This corresponds to the excitation from E4, the highest energy level of ground state manifold, to E5, the lowest energy level of the excited state manifold. By resonantly exciting electrons from  ${}^2F_{7/2}$  to  ${}^2F_{5/2}$  with the lowest energy photons, the traditional method maximize the  $\lambda/\tilde{\lambda}(T)$ . This is an ideal protocol when the absorption coefficient ( $\alpha$ ) is much larger than the background absorption coefficient ( $\alpha_b$ ), which is not the case for 1020 nm photons when the internal temperature is below 100 K.

Without Purcell enhancement, we calculated the cooling efficiency as a function of temperature at the optimum pump wavelength of 1020 nm, shown in Fig. 1(d). The calculation is based on experimental measured flu-

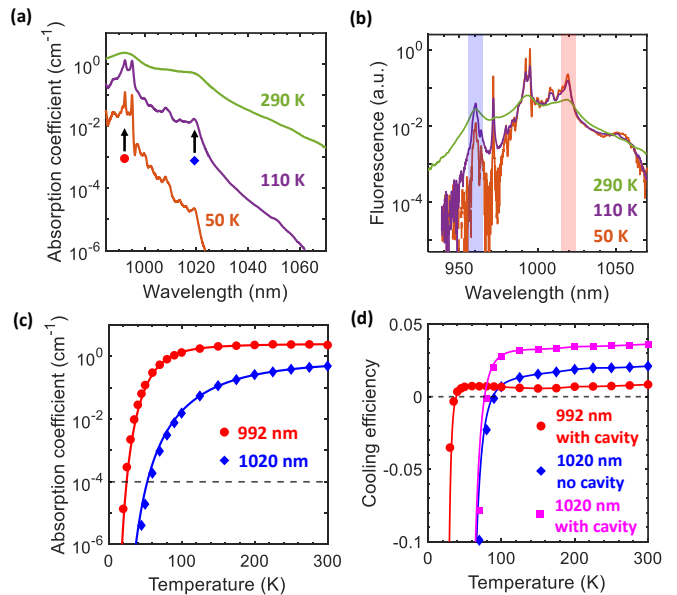


FIG. 2. (a) Absorption coefficient of 5%  $\text{Yb}^{3+}:\text{YLF}$  at different temperatures for pi-polarization. The brown, purple, and green curves corresponds to the absorption spectra at 50 K, 110 K, and 290 K. The red dot and blue diamond indicates the absorption peaks near 992 nm and 1020 nm. (b) Measured emission spectra of 5%  $\text{Yb}^{3+}:\text{YLF}$  at different temperatures. The brown, purple and green curves corresponds to the measured emission spectra at 50 K, 110 K, and 290 K. The red and blue spectrum ranges indicate the emission bands from E5 to E4 and from E6 to E1, respectively. (c) Measured absorption coefficient of  $\text{Yb}^{3+}:\text{YLF}$  as a function of temperature at 992 nm and 1020 nm represented by red dots and blue diamonds, respectively. The red and blue curves correspond to the fitting curves of the measured data. The black dashed line indicates the background absorption coefficient  $\alpha_b$ . (d) Calculated cooling efficiency as a function of temperature. The red dots show the cooling efficiency for optical pumping at 992 nm with cavity-induced Purcell enhancement. The blue diamonds show the cooling efficiency for optical pumping at 1020 nm without cavity. The magenta squares shows cooling efficiency for optical pumping at 1020 nm with cavity-induced Purcell enhancement. The red, blue and magenta solid curves are the corresponding calculated results based on the fitting curves in (c).

orescence spectra of 5%  $\text{Yb}^{3+}:\text{YLF}$  at different temperatures. Details of the calculation is shown in the supplementary material, where we assume  $\eta_{\text{ext}} = 0.996$  and  $\alpha_b = 10^{-4} \text{ cm}^{-1}$  [20]. Without Purcell enhancement, the MAT is about 94 K. This is close to the MAT obtained by state-of-the-art experimental optical refrigeration of  $\text{Yb}^{3+}:\text{YLF}$  crystal [19, 20].

In our proposed optical refrigeration protocol (Fig. 1(e)), the cavity enhances the zero phonon line emission at 972 nm with Purcell effect and blue shift the mean emission wavelength (Fig. S1(b)). This allows us to excite the absorption peak at 992 nm, which shows an absorption coefficient larger than  $1 \text{ cm}^{-1}$  at 100 K. The

calculated cooling efficiency as a function of temperature and the pump wavelength is shown as Fig. 1(f). The MAT of  $\text{Yb}^{3+}:\text{YLF}$  crystal is reduced as a result of the increased absorption coefficient and the blueshift of mean emission wavelength, as shown in the Fig. S1(a). In particular, the MAT is 38 K when pumped at the optimum wavelength of 992 nm. The dramatic improvement on the MAT with our protocol can potentially enable many applications that require cooling below  $\text{LN}_2$  temperature [21, 22]. In addition to the significantly improved MAT, optical refrigeration below  $\text{LN}_2$  temperature can be achieved by absorbing a broad band of photons between 987 nm and 1010 nm, making optical refrigeration an accessible substitute of liquid nitrogen cooling system.

Fig. 2(a) and 2(b) show the calculated absorption coefficient spectra based on reciprocity relation and the measured fluorescence spectra of the 5%  $\text{Yb}^{3+}:\text{YLF}$  crystal at different temperatures, respectively. Both absorption and emission spectra have narrower peaks at lower temperatures due to the reduced thermal crystal phonon energy. The population distribution of the excited state manifold of  $\text{Yb}^{3+}:\text{YLF}$  follows the Boltzmann distribution. The red and blue spectrum range in Fig. 2(b) corresponds to the emission band from E5 to E4 and from E6 to E1, respectively. Therefore, the fluorescence ratio between blue band and red band can be used to characterize the internal temperature of the  $\text{Yb}^{3+}:\text{YLF}$  nanocrystal, as shown in Fig. S2(a).

Higher absorption coefficient at 992 nm than 1020 nm significantly enhances the cooling efficiency of  $\text{Yb}^{3+}:\text{YLF}$  nanocrystal. As shown in Fig. 2(c), the measured absorption coefficient at 992 nm is over 50 times larger than the absorption coefficient at 1020 nm when the temperature is 100 K. This ratio increases at lower temperatures. At the temperature of 50 K,  $\eta_{\text{abs}}(50 \text{ K}, 1020 \text{ nm})$  drops to around 0.5 while  $\eta_{\text{abs}}(50 \text{ K}, 992 \text{ nm})$  remains nearly unity, which is critical for efficient cooling. The decreased absorption coefficient of 1020 nm is caused by population depletion of E4 state (Fig. 1(c)) at low temperatures. According to the Boltzmann distribution, the population of E2 states (Fig. 1(e)) with lower energy is exponentially larger at the same temperature, leading to larger absorption coefficient at 992 nm. Our finding indicates that nanocrystal with lower E2 energy, such as  $\text{Yb:KY}_3\text{F}_{10}$  [35], can potentially achieve lower MAT with our proposed optical refrigeration protocol.

Fig. 2(d) shows the cooling efficiency of different optical refrigeration methods calculated from equation (1). Without cavity, the cooling efficiency is limited by  $\frac{k_B T}{hc/\lambda}$  [2]. Cavity-induced Purcell enhancement can significantly increase the cooling efficiency beyond this limit. Despite enhanced cooling power, the MAT is constrained by the vanishing absorption coefficient of 1020 nm photons at low temperatures, as shown in Fig. 2(d). In addition to Purcell enhanced emission, our proposed method utilized the optimized pumping wavelength of 992 nm

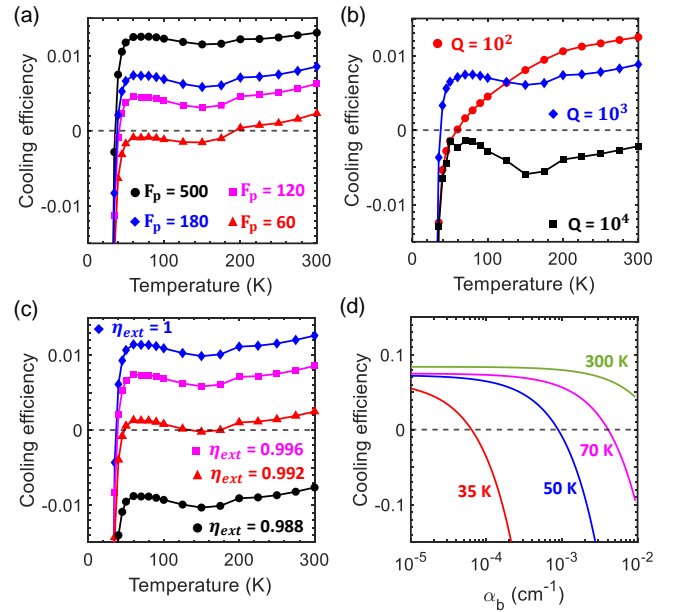


FIG. 3. Investigate the impact of experimental conditions on the proposed Purcell enhanced optical refrigeration protocol. (a) Cooling efficiency as a function of temperature for different  $F_p$  as a result of different separation between the  $\text{Yb}^{3+}:\text{YLF}$  nanocrystal and the cavity. (b) Cooling efficiency as a function of temperature for different Q factors of the photonic nanocavity. (c) Cooling efficiency as a function of temperature for different external quantum efficiency ( $\eta_{\text{ext}}$ ) of the  $\text{Yb}^{3+}:\text{YLF}$  nanocrystal. (d) Cooling efficiency as a function of the background absorption coefficient ( $\alpha_b$ ) of the  $\text{Yb}^{3+}:\text{YLF}$  nanocrystal for different temperatures.

by considering the trade-off between per-photon cooling power and absorption coefficient. The calculated cooling efficiency is nearly constant for temperatures above 50 K, making this an ideal method for optical refrigeration below the  $\text{LN}_2$  temperature. In practice, both high cooling efficiency at high temperature and low MAT can be achieved by switching pumping laser from 1020 nm to 992 nm at 70 K. Our protocol can easily be adapted to enhance the optical refrigeration of other rare-earth doped particles.

To study the experimental feasibility of the proposed protocol, we calculated the cooling efficiency of  $\text{Yb}^{3+}:\text{YLF}$  nanocrystal in various experimental conditions. Besides the intrinsic properties of  $\text{Yb}^{3+}$  such as fluorescence, absorption, and energy structure, the properties of cavity and YLF nanocrystal strongly affect the Purcell enhanced cooling efficiency. The  $F_p$  at the location of the nanocrystal and the cavity Q factor collaboratively determines Purcell enhanced emission of high energy photons, therefore, strongly affects the cooling efficiency.

The  $F_p$  at the location of nanocrystal depends on the design of the cavity as well as the separation between

the nanocrystal and the center of the cavity [33, 34]. Our former calculation is based on a moderate  $F_p = 180$ . As shown in Fig. 3(a), while increasing the Purcell factor beyond  $F_p = 120$  enhances the cooling efficiency, this change has limited effect on the MAT. The Q factor of the cavity determines the wavelength range that is enhanced by the Purcell effect (See supplementary materials for more information). To optimize MAT, the linewidth of the cavity should match with the linewidth of the zero-phonon emission peak. For this reason,  $Q = 1000$  leads to the better cooling effect than larger or smaller Q, as shown in Fig. 3(b).

Improving the purity of the material has been the focus for achieving cryogenic cooling with  $\text{Yb}^{3+}:\text{YLF}$  crystals. In the past few decades, great progress has made to synthesize high purity  $\text{Yb}^{3+}:\text{YLF}$  with near unity quantum efficiency and a remarkable low background absorption coefficient of about  $10^{-4} \text{ cm}^{-1}$  [20]. From Fig. 3(d), the cooling efficiency at 50 K remains positive for  $\alpha_b$  up to  $8.7 \times 10^{-4} \text{ cm}^{-1}$ . While further improving  $\alpha_b$  is required for achieving positive cooling below 38 K, the above analysis shows that our proposed Purcell enhanced optical refrigeration method is able to achieve cooling below  $\text{LN}_2$  temperature with realistic experimental conditions.

In the paper, we proposed a novel Purcell enhanced optical refrigeration protocol. For a  $\text{Yb}^{3+}:\text{YLF}$  nanocrystal near a cavity, the minimum achievable temperature is predicted to be 38 K based on measured fluorescence spectra. A complete study of the protocol is conducted over various experimental conditions of cavity and nanocrystal, validating the feasibility of the method. Our protocol paves the way for various applications of optical refrigeration below  $\text{LN}_2$  temperatures and can be adopted to improve the MAT of several solid-state coolers [15, 35].

We thank Chen-Lung Hung, Xinchao Zhou, Peter J Pauzauskie for helpful discussions. We acknowledge the support from the Office of Naval Research under Grant No. N00014-18-1-2371 and National Science Foundation under Grant PHY-2110591.

---

\* [tcli@purdue.edu](mailto:tcli@purdue.edu)

- [1] M. Sheik-Bahae and R. I. Epstein, Optical refrigeration, *Nature Photonics* **1**, 693 (2007).
- [2] D. V. Seletskiy, R. Epstein, and M. Sheik-Bahae, Laser cooling in solids: advances and prospects, *Reports on Progress in Physics* **79**, 096401 (2016).
- [3] R. I. Epstein, M. I. Buchwald, B. C. Edwards, T. R. Gosnell, and C. E. Mungan, Observation of laser-induced fluorescent cooling of a solid, *Nature* **377**, 500 (1995).
- [4] J. Zhang, D. Li, R. Chen, and Q. Xiong, Laser cooling of a semiconductor by 40 Kelvin, *Nature* **493**, 504 (2013).
- [5] B. Topper, S. Kuhn, A. Neumann, A. R. Albrecht, A. S. Flores, D. Hässner, S. Hein, C. Hupel, J. Nold, N. Haarlammert, T. Schreiber, M. Sheik-Bahae, and A. Mafi, Laser cooling ytterbium doped silica by 67 K from ambient temperature, *Opt. Express* **32**, 3660 (2024).
- [6] C. W. Hoyt, M. P. Hasselbeck, M. Sheik-Bahae, R. I. Epstein, S. Greenfield, J. Thiede, J. Distel, and J. Valencia, Advances in laser cooling of thulium-doped glass, *J. Opt. Soc. Am. B* **20**, 1066 (2003).
- [7] S. Rostami, A. R. Albrecht, A. Volpi, and M. Sheik-Bahae, Observation of optical refrigeration in a holmium-doped crystal, *Photon. Res.* **7**, 445 (2019).
- [8] A. T. M. A. Rahman and P. F. Barker, Laser refrigeration, alignment and rotation of levitated  $\text{Yb}^{3+}:\text{YLF}$  nanocrystals, *Nature Photonics* **11**, 634 (2017).
- [9] M. Hua and R. S. Decca, Net energy up-conversion processes in  $\text{CdSe}/\text{CdS}$  (core/shell) quantum dots: A possible pathway towards optical cooling, *Phys. Rev. B* **106**, 085421 (2022).
- [10] A. Pant, X. Xia, E. J. Davis, and P. J. Pauzauskie, Solid-state laser refrigeration of a composite semiconductor  $\text{Yb}:\text{YLiF}_4$  optomechanical resonator, *Nature Communications* **11**, 3235 (2020).
- [11] S. Dadras, K. Shayan, D. R. Luntz-Martin, R. G. Felsted, P. J. Pauzauskie, and A. N. Vamivakas, Thermometry of solid-state laser refrigeration using NV- centers in nanodiamonds, in *OSA Quantum 2.0 Conference* (Optica Publishing Group, 2020) p. QW6A.18.
- [12] M. P. Hehlen, J. Meng, A. R. Albrecht, E. R. Lee, A. Gragossian, S. P. Love, C. E. Hamilton, R. I. Epstein, and M. Sheik-Bahae, First demonstration of an all-solid-state optical cryocooler, *Light: Science & Applications* **7**, 15 (2018).
- [13] J. L. Kock, A. R. Albrecht, R. I. Epstein, and M. Sheik-Bahae, Optical refrigeration of payloads to < 125 K, *Opt. Lett.* **47**, 4720 (2022).
- [14] P. B. Roder, B. E. Smith, X. Zhou, M. J. Crane, and P. J. Pauzauskie, Laser refrigeration of hydrothermal nanocrystals in physiological media, *Proceedings of the National Academy of Sciences* **112**, 15024 (2015).
- [15] D. R. Luntz-Martin, R. G. Felsted, S. Dadras, P. J. Pauzauskie, and A. N. Vamivakas, Laser refrigeration of optically levitated sodium yttrium fluoride nanocrystals, *Opt. Lett.* **46**, 3797 (2021).
- [16] C. Laplane, P. Ren, R. P. Roberts, Y. Lu, and T. Volz, Inert shell coating for enhanced laser refrigeration of nanoparticles: Application in levitated optomechanics, *ACS Photonics* **11**, 963 (2024).
- [17] J. Ahn, Z. Xu, J. Bang, P. Ju, X. Gao, and T. Li, Ultrasensitive torque detection with an optically levitated nanorotor, *Nature Nanotechnology* **15**, 89 (2020).
- [18] U. Delić, M. Reisenbauer, K. Dare, D. Grass, V. Vuletić, N. Kiesel, and M. Aspelmeyer, Cooling of a levitated nanoparticle to the motional quantum ground state, *Science* **367**, 892 (2020).
- [19] A. Volpi, J. Meng, A. Gragossian, A. R. Albrecht, S. Rostami, A. D. Lieto, R. I. Epstein, M. Tonelli, M. P. Hehlen, and M. Sheik-Bahae, Optical refrigeration: the role of parasitic absorption at cryogenic temperatures, *Opt. Express* **27**, 29710 (2019).
- [20] S. D. Melgaard, A. R. Albrecht, M. P. Hehlen, and M. Sheik-Bahae, Solid-state optical refrigeration to sub-100 Kelvin regime, *Scientific Reports* **6**, 20380 (2016).
- [21] B. Keimer, S. A. Kivelson, M. R. Norman, S. Uchida, and J. Zaanen, From quantum matter to high-temperature superconductivity in copper oxides, *Nature* **518**, 179 (2015).

- [22] A. Gottscholl, M. Diez, V. Soltamov, C. Kasper, A. Sperlich, M. Kianinia, C. Bradac, I. Aharonovich, and V. Dyakonov, Room temperature coherent control of spin defects in hexagonal boron nitride, *Science Advances* **7**, eabf3630 (2021).
- [23] M. Notomi, Manipulating light with strongly modulated photonic crystals, *Reports on Progress in Physics* **73**, 096501 (2010).
- [24] B. Romeira and A. Fiore, Purcell effect in the stimulated and spontaneous emission rates of nanoscale semiconductor lasers, *IEEE Journal of Quantum Electronics* **54**, 1 (2018).
- [25] L. Yang, S. Wang, M. Shen, J. Xie, and H. X. Tang, Controlling single rare earth ion emission in an electro-optical nanocavity, *Nature Communications* **14**, 1718 (2023).
- [26] B. Casabone, C. Deshmukh, S. Liu, D. Serrano, A. Ferrier, T. Hümmer, P. Goldner, D. Hunger, and H. de Riedmatten, Dynamic control of purcell enhanced emission of erbium ions in nanoparticles, *Nature Communications* **12**, 3570 (2021).
- [27] J. D. Thompson, T. G. Tiecke, N. P. de Leon, J. Feist, A. V. Akimov, M. Gullans, A. S. Zibrov, V. Vuletić, and M. D. Lukin, Coupling a single trapped atom to a nanoscale optical cavity, *Science* **340**, 1202 (2013).
- [28] T. G. Tiecke, J. D. Thompson, N. P. de Leon, L. R. Liu, V. Vuletić, and M. D. Lukin, Nanophotonic quantum phase switch with a single atom, *Nature* **508**, 241 (2014).
- [29] P. Ju, Y. Jin, K. Shen, Y. Duan, Z. Xu, X. Gao, X. Ni, and T. Li, Near-field GHz rotation and sensing with an optically levitated nanodumbbell, *Nano Letters* **23**, 10157 (2023).
- [30] L. Magrini, R. A. Norte, R. Riedinger, I. Marinković, D. Grass, U. Delić, S. Gröblacher, S. Hong, and M. Aspelmeyer, Near-field coupling of a levitated nanoparticle to a photonic crystal cavity, *Optica* **5**, 1597 (2018).
- [31] Y. Feng, Y. Sato, T. Inoue, M. Liu, S. Chiashi, R. Xiang, K. Suenaga, and S. Maruyama, Drastically reduced thermal conductivity of self-bundled single-walled carbon nanotube, *Carbon* **201**, 433 (2023).
- [32] S. Püschel, S. Kalusniak, C. Kränkel, and H. Tanaka, Temperature-dependent radiative lifetime of Yb:YLF: refined cross sections and potential for laser cooling, *Opt. Express* **29**, 11106 (2021).
- [33] M. Albrechtsen, B. Vosoughi Lahijani, R. E. Christiansen, V. T. H. Nguyen, L. N. Casse, S. E. Hansen, N. Stenger, O. Sigmund, H. Jansen, J. Mørk, and S. Stobbe, Nanometer-scale photon confinement in topology-optimized dielectric cavities, *Nature Communications* **13**, 6281 (2022).
- [34] G. Kountouris, J. Mørk, E. V. Denning, and P. T. Kristensen, Modal properties of dielectric bowtie cavities with deep sub-wavelength confinement, *Opt. Express* **30**, 40367 (2022).
- [35] S. Püschel, F. Mauerhoff, C. Kränkel, and H. Tanaka, Laser cooling in Yb:KY3F10: a comparison with Yb:YLF, *Opt. Express* **30**, 47235 (2022).